Following the Growth Process in Macroporous Methylsilsesquioxane Films at the Single Macropore Level by Confocal Correlation Spectroscopy

Hanjiang Dong,[†] Fangmao Ye,[†] Daniel A. Higgins,*[,†] and Maryanne M. Collinson*[,‡]

Department of Chemistry, Kansas State University, Manhattan, Kansas 66506, and Department of Chemistry, Virginia Commonwealth University, 1001 West Main St., Richmond, Virginia 23284

Received August 22, 2007. Revised Manuscript Received October 19, 2007

Optical microscopy and in situ single pore confocal correlation spectroscopy (CCS) were used to study the evolution of macroporous methylsilsesquioxane (MSQ) films formed by the acid-catalyzed hydrolysis and condensation of methyltrimethoxysilane. Spinodal decomposition and gelation in the films were directly observed using these methods. Phase separation was found to occur 5 h 40 min after sol preparation, followed by gelation at 6 h 50 min. MSQ "nanoparticles" appeared in the films very early after sol preparation. These nanoparticles produced bursts of elastically scattered light as they passed through the detection volume. Detailed information on nanoparticle growth was obtained by recording single point time transients in the sol film and in individual pores of the phase-separated and gelled matrix. Apparent diffusion coefficients and average nanoparticle sizes were obtained by fitting autocorrelations of the time transient data to an appropriate expression. The nanoparticles were found to grow rapidly to a maximum diameter of ~30 nm and to remain in this size range until well after gelation of the matrix. Nanoparticle size stabilization was attributed to consumption of reactive species and to changes in nanoparticle surface reactivity brought about by the condensation process. Beginning soon after gelation, incorporation of the nanoparticles in/on the matrix was evidenced by a decrease in the number of particles present in the pores. After a delay of ~3 h, nanoparticle growth within the pores resumed, as exhibited by a decrease in their apparent diffusion coefficients. Nanoparticle growth in this later phase was attributed to aggregation of nonpolar MSQ particles.

Introduction

Macroporous sol–gel-derived monoliths and films represent an intriguing class of materials that have attracted considerable attention recently owing to their unique structural features and potential applications as catalyst supports, stationary phases for chemical separations, superhydrophobic materials, and as materials for drug delivery, chemical sensors, and optics.[1–6] One common method for preparing these materials is by polymerization-induced phase separation (i.e., spinodal decomposition) in silicon–alkoxide-derived sols.[7] Methyltrimethoxysilane (MTMOS) represents an important example of the silicon–alkoxide precursors that have been employed in recent synthetic studies.[2,3,8–12] Hydrolysis and condensation of MTMOS in acidic water–methanol mixtures leads to formation of relatively nonpolar methylsilsesquioxane (MSQ) oligomers and polymers.[13] Under appropriate conditions, MTMOS-derived MSQ polymers can spontaneously phase separate from the water–methanol solution,[2,9] forming a two-phase system. Importantly, phase separation can occur without the use of additives (i.e., organic polymers).[1] Subsequent gelation converts the phase-separated sol to a rigid, porous matrix. Pore size and overall materials morphology can easily be controlled by simply varying the time between phase separation and gelation.[7] These same MSQ-based materials prepared under slightly different conditions can also yield homogeneous sols, precipitates, or resins.[2,8] The diversity of materials that can be obtained results in part from the complexity of the phase separation and sol–gel transition processes.

A variety of methods such as NMR, XRD, light scattering, SAXS, confocal microscopy, electron microscopy, and porosimetry have been used previously to follow the sol–gel process in pore-forming and related systems and to probe the chemical and physical properties of the resulting

* Corresponding authors. E-mail: higgins@ksu.edu, mmcollinson@vcu.edu.
[†] Kansas State University.
[‡] Virginia Commonwealth University.

(1) Nakanishi, K.; Kanamori, K. *J. Mater. Chem.* **2005**, *15*, 3776–3786.
(2) Dong, H.; Brook, M. A.; Brennan, J. D. *Chem. Mater.* **2005**, *17*, 2807–2816.
(3) Shea, K. J.; Loy, D. A. *Chem. Mater.* **2001**, *13*, 3306–3319.
(4) Hartmann, S.; Brandhuber, D.; Hüsing, N. *Acc. Chem. Res.* **2007**, *40*, 885–894.
(5) Shirtcliffe, N. J.; McHale, G.; Newton, M. I.; Perry, C. C. *Langmuir* **2003**, *19*, 5626–5631.
(6) Yuan, Z.-Y.; Su, B.-L. *J. Mater. Chem.* **2006**, *16*, 663–667.
(7) Nakanishi, K. *J. Porous Mater.* **1997**, *4*, 67–112.
(8) Loy, D. A.; Baugher, B. M.; Baugher, C. R.; Schneider, D. A.; Rahimian, K. *Chem. Mater.* **2000**, *12*, 3624–3632.
(9) Dong, H.; Brennan, J. D. *Chem. Mater.* **2006**, *18*, 4176–4182.
(10) Dong, H.; Brennan, J. D. *Chem. Mater.* **2006**, *18*, 541–546.
(11) Dong, H.; Lee, M.; Thomas, R. D.; Zhang, Z.; Reidy, R. F.; Mueller, D. W. *J. Sol-Gel Sci. Technol.* **2003**, *28*, 5–14.
(12) Dong, H.; Zhang, Z.; Lee, M.-H.; Mueller, D. W.; Reidy, R. F. *J. Sol-Gel Sci. Technol.* **2007**, *41*, 11–17.
(13) Baney, R. H.; Itoh, M.; Sakakibara, A.; Suzuki, T. *Chem. Rev.* **1995**, *95*, 1409–1430.
(14) Devreux, F.; Boilot, J. P.; Chaput, F.; Lecomte, A. *Phys. Rev. A* **1990**, *41*, 6901–6909.

10.1021/cm702382c CCC: $37.00
Published on Web 11/22/2007

materials.[1,4,7–9,11–20] Unfortunately, few of these (e.g., NMR, light scattering, SAXS, confocal microscopy) are capable of following real time changes during the sol–gel transition. The others (e.g., XRD, electron microscopy, porosimetry) can only be used to probe dried materials. NMR, while invaluable as a means to determine the molecular species present, has not yet been used to probe the sol–gel process in phase-separated systems, likely because of sample inhomogeneity. Although laser scanning confocal microscopy has been used to image the *static* three-dimensional structures within macroporous sol–gel materials,[1,19,20] only aged wet gels and dried gels have been investigated. While conventional bulk light scattering methods have provided a wealth of information on the time evolution of such materials,[7,15] these methods primarily probe regions of high polymer concentration (the matrix, after phase separation and gelation have occurred). Importantly, the sol–gel dynamics in regions of low polymer content (the macropores) have not previously been directly probed by these or any other methods. As the silica, catalyst, and solvent concentrations differ spatially within all these materials, a full understanding of their formation and aging can only be obtained by probing the dynamics in a spatially resolved manner.

In this paper, an in situ microscopic technique, confocal correlation spectroscopy (CCS),[21] is used to follow the polymerization of MTMOS films from before phase separation to well after gelation. Implementation of optical microscopic methods allows for the different phases (i.e., pores and matrix) to be distinguished from each other and separately probed with submicrometer-scale spatial resolution in real time. Light scattering by the individual MSQ "nanoparticles" that appear in the sol (before phase separation) or within the pores (after phase separation) is used as a means to follow the time evolution of these materials. Conceptually, CCS is similar to fluorescence correlation spectroscopy,[22] commonly used by our groups[23,24] and others[25–27] to study sol–gel-derived materials. However, because no dyes are employed in the present studies, the structural evolution of the individual sol–gel-derived particles that ultimately come together to form the matrix may be probed without concern for the effects of dye partitioning and dye–matrix interactions.

Experimental Section

Sample Preparation. All chemicals employed, including methyltrimethoxysilane (MTMOS, >98%), nitric acid (HNO_3), water (HPLC grade), and methanol (MeOH, HPLC grade), were obtained from Aldrich and were used as received. Bulk samples were prepared using a procedure modified from the literature.[28] Briefly, 0.50 mL of MTMOS and 0.14 mL of MeOH were first mixed in a small vial. After 5 min, 0.13 mL of 1 M HNO_3 was quickly added. The mixture was then vigorously agitated for 1 min at room temperature. The final mole ratios of Si:H_2O:MeOH were 1:2:1.

Preparation of MSQ films for use in the CCS studies was performed 20 min after preparation of the sol. In this procedure, a 1.5 μL aliquot of the sol was dropped onto the center of a microscope cover slide. The slide was then quickly covered with a second cover glass to spread the sol and to prevent its evaporation. The films obtained were determined to be 2–5 μm thick by optical microscopy (see below).

Optical Microscopy. Samples prepared by the above procedure were immediately transferred to a sample scanning confocal microscope for imaging and for the recording of time transients. All experiments were performed under ambient laboratory conditions, with the top cover slide in place. The microscope employed has been described previously in detail.[29] Briefly, it is comprised of an inverted light microscope, upon which is mounted a closed-loop piezoelectric *X*,*Y* scanning stage. In the present experiments, the microscope was used in the epi-illumination mode to selectively collect and detect 543.5 nm laser light scattered by the sample matrix and by MSQ particles within the film and pores. Incident light (<3 μW) was delivered to the sample using a high numerical aperture (NA = 1.3) oil-immersion objective. A dichroic mirror (Chroma Technologies 565DCLP) was used to direct the laser light into the back aperture of this objective. The same objective was used to collect light scattered by the sample. Light collected from the sample subsequently passed through the dichroic mirror and into the detection path. The dichroic mirror served to reduce the intensity of the scattered light into the linear range of the single-photon-counting avalanche photodiode detector.[30] Pulses from the detector were counted using a National Instruments counter-timer card (PCI-6602).

Other Characterization Methods. SEM images were obtained using a Hitachi S-3500N SEM with an acceleration voltage of 20 kV. The surfaces of the samples were coated with ~50 Å of gold before imaging by SEM. Optical density data from the bulk sols were obtained at a wavelength of 543.5 nm, using a HP 8453 diode array spectrometer. Film thickness was obtained using the optical microscope described above. For this purpose, the incident laser light was alternately focused on the glass/sol interfaces of the upper and lower cover glasses. The distance between these two foci was read from the calibrated scale on the microscope focal knob and was recorded as the film thickness.

Results and Discussion

Imaging of Macroporous MSQ Films. A variety of different materials, including homogeneous and phase-separated

(15) Kaji, H.; Nakanishi, K.; Soga, N.; Inoue, T.; Nemoto, N. *J. Sol-Gel. Sci. Technol.* **1994**, *3*, 169–188.
(16) Sanchez, J.; Rankin, S. E.; McCormick, A. V. *Ind. Eng. Chem. Res.* **1996**, *34*, 117–129.
(17) Rankin, S. E.; Macocko, C. W.; McCormick, A. V. *AIChE J.* **1998**, *44*, 1141–1156.
(18) Smått, J.-H.; Schunk, S.; Lindén, M. *Chem. Mater.* **2003**, *15*, 2354–2361.
(19) Kanamori, K.; Nakanishi, K.; Hirao, K.; Jinnai, H. *Langmuir* **2003**, *19*, 5581–5585.
(20) Kanamori, K.; Ishizuka, N.; Nakanishi, K. *J. Sol-Gel. Sci. Technol.* **2003**, *26*, 157–160.
(21) Kuyper, C. L.; Budzinski, K. L.; Lorenz, R. M.; Chiu, D. T. *J. Am. Chem. Soc.* **2006**, *128*, 730–731.
(22) Elson, E. L.; Magde, D. *Biopolymers* **1974**, *13*, 1–27.
(23) Ye, F.; Higgins, D. A.; Collinson, M. M. *J. Phys. Chem. C* **2007**, *111*, 6772–6780.
(24) Fu, Y.; Ye, F.; Sanders, W. G.; Collinson, M. M.; Higgins, D. A. *J. Phys. Chem. B* **2006**, *110*, 9164–9170.
(25) Seebacher, C.; Hellriegel, C.; Deeg, F.-W.; Brauchle, C.; Altmaier, S.; Behrens, P.; Müllen, K. *J. Phys. Chem. B* **2002**, *106*, 5591–5595.
(26) Mahurin, S. M.; Dai, S.; Barnes, M. D. *J. Phys. Chem. B* **2003**, *107*, 13336–13340.
(27) McCain, K. S.; Hanley, D. C.; Harris, J. M. *Anal. Chem.* **2003**, *75*, 4351–4359.
(28) Kanamori, K.; Yonezawa, H.; Nakanishi, K.; Hirao, K.; Jinnai, H. *J. Sep. Sci.* **2004**, *27*, 874–886.
(29) Higgins, D. A.; Collinson, M. M.; Saroja, G.; Bardo, A. M. *Chem. Mater.* **2002**, *14*, 3734–3744.
(30) Kuyper, C. L.; Fujimoto, B. S.; Zhao, Y.; Schiro, P. G.; Chiu, D. T. *J. Phys. Chem. B* **2006**, *110*, 24433–24441.

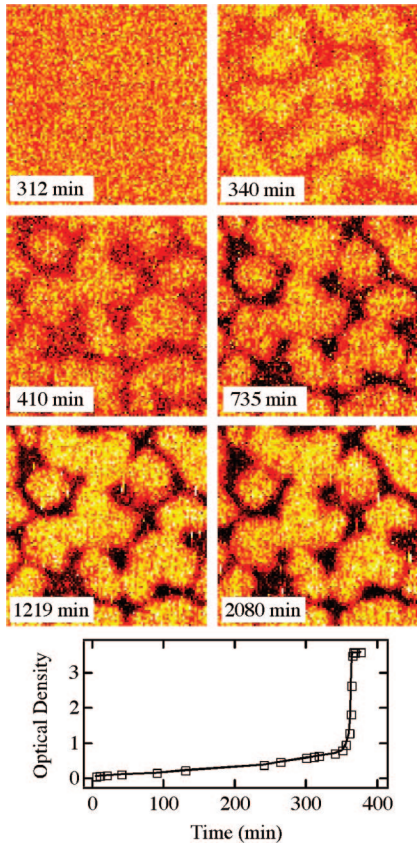

Figure 1. Optical images (top, 10 × 10 μm^2) of an MSQ film as a function of time after sol preparation. Prior to phase separation (<340 min) the film uniformly scatters light. At 340 min, the sol undergoes a spinodal decomposition and a two-phase system appears. The bright regions are the matrix (high silica concentration) and the dark regions the pores (low silica concentration). The two phases continue to evolve (i.e., they remain mobile) until sometime after the gel transition in the film (>410 min). Beyond 735 min, the film structure is observed to be stable, although the optical contrast between matrix and pores continues to improve. Optical density (bottom) at 543 nm as a function of time obtained from the associated bulk gel. These data show that phase separation occurs at approximately the same time in the bulk gel and the film. Gelation occurs in the bulk gel at 405 min.

sols and gels, can be prepared when MTMOS is hydrolyzed and condensed.[2] The type of material formed depends on the Si:water ratio, the catalyst, the pH of the sol, and whether a one-step or two-step polymerization procedure is employed.[2,9,10] In contrast to what was believed a decade ago, it has recently been shown that gels can be formed from MTMOS sols when the pH is very low.[1,2] In the present work, the Si:water ratio was 1:2, just above the stoichiometric requirement, and the sols were highly acidic (pH ∼ 1). Under these conditions, both phase separation and gel formation occur.

Optical images of the films prepared as described above provide a detailed view of MSQ film evolution from before phase separation to well after gelation. Figure 1 shows representative examples of the images obtained. The signal at each pixel in these 100 × 100 pixel images was integrated for 40 ms. Spectra of the light collected proved that elastic scattering by the sample was the dominant source of signal and optical contrast in all such images. Also shown in Figure 1 is the time-dependent optical density of the bulk sol from which this film was prepared. These latter data were recorded from just after sol preparation until just after phase separation.

At early times (i.e., for a period of more than 5 h), no distinct features are observed in the optical images. However, all such images yield signals larger than the dark background of the microscope. As noted above, these signals arise from light scattering by the sol. Here, light scattering is specifically attributed to scattering by MSQ "nanoparticles". The presence of these nanoparticles is supported by the gradual increase in optical density observed for the bulk sol (see Figure 1) at early times. SEM data obtained from gelled films (see below) provide further evidence of their existence. The formation of such particles is also well-known from previous SAXS studies of similar materials.[31] However, the nanoparticles formed at early times are not likely to be true solid particles of well-defined shape. Rather, they likely consist of weakly cross-linked (i.e., low density) MSQ oligomers having optical properties that differ only modestly from the solvent (i.e., methanol).

Phase separation (i.e., spinodal decomposition) is observed to occur in this film just prior to 5 h 40 min (340 min), as evidenced by formation of a two-phase system at this point (see Figure 1). The two phases consist of regions high in MSQ polymer concentration (bright regions exhibiting relatively strong light scattering) and those that are low in MSQ concentration (dark regions exhibiting relatively weak scattering). It should be noted that the time at which phase separation occurs is defined here as the first appearance of a two-phase system in the optical microscope. In previous reports, phase separation has often been defined as the time at which the sol just begins to turn turbid.[28] Here, the plot of optical density vs time for the bulk sol (Figure 1) provides this information. In this plot, the optical density is observed to gradually increase for more than the first 5 h. It then abruptly rises at 5 h 50 min (350 min), a time that is consistent with the phase separation time deduced from the optical images. These data suggest that there is little difference in the hydrolysis and condensation processes of the bulk sols and films studied here. Similarities between these samples are not surprising since the micron thick films are really "thin monoliths" that are also kept covered (like the bulk samples) to minimize evaporation.

After phase separation but prior to gelation, the regions of high and low MSQ concentration continue to evolve in size, shape, and position, as evidenced by the images shown in Figure 1. The time between phase separation and gelation is one of the most important factors governing the final morphology of these macroporous materials.[7] At the gelation point, the regions of high MSQ concentration rapidly form a rigid, permanent structure: the "matrix". The regions of low MSQ concentration become the "pores" of the matrix and are filled primarily with liquid solvent at this point.

The time at which gelation occurs can also be deduced from the images shown in Figure 1. In this particular sample, the size and shape of the individual regions show little change after 6 h 50 min (compare images recorded at 410, 735, 1219, and 2080 min). Therefore, this is concluded to be the approximate time of film gelation. The film gelation time closely corresponds to the 6 h 45 min (405 min) gelation

(31) Boukari, H.; Lin, J. S.; Harris, M. T. *Chem. Mater.* **1997**, *9*, 2376–2384.

time observed in the bulk sample. Gelation was detected in the bulk sample by observation of a dramatic change in sol viscosity.

The optical images obtained after gelation indicate the films are comprised of pores having 1–2 μm cross-sectional dimensions. Because they are interconnected, the pores often appear as "channels" with lengths in excess of 10 μm. The pores are separated from each other by regions of solid MSQ matrix that, on average, are similar in size to the pores. Convolution of physical matrix structures with the ~300 nm $1/e^2$ radius of the Gaussian laser profile used to image the samples causes some broadening of the image features.

As a final observation from the optical images (Figure 1), it should be noted that while the pore and matrix structures become fixed at the time of gelation, the optical contrast between these regions continues to increase for many hours. This observation is consistent with the continued evolution of the chemical and physical properties of these regions. Specifically, increased light scattering from the matrix reflects its continued densification and a corresponding increase in its refractive index (relative to that of the solvent-filled pores). Likewise, a steady reduction in overall light scattering observed from the pores reflects time-dependent changes in the number of MSQ nanoparticles present. Light scattering from the pores is primarily manifested as bright vertical "streaks" in the optical images (see Figure 1). These results indicate light scattering from the pores is dominated by "random" passage of mobile MSQ nanoparticles through the focal volume of the microscope. It is noteworthy that the brightness of these steaks increases in time, consistent with continued growth and densification of the nanoparticles long after gelation has occurred.

Higher resolution images of the MSQ films were obtained by SEM. Figure 2 shows representative examples. These images provide further support for the above conclusions pertaining to film morphology and composition. Both images were obtained from the film shown in Figure 1, although the areas imaged are different. SEM images provide a good picture of the final structure of *dried* macroporous MSQ materials, but they provide no information on the time evolution of the film structure. The features observed are also potentially altered from their original state during the drying process. However, the optical and SEM images provide a consistent view of the matrix and pores. The SEM image shown in Figure 2A depicts round and oblong interconnected pores. The smallest pores observed at this magnification are 1–2 μm in size, while larger pores having widths on the order of 5–10 μm and lengths of more than 50 μm are also frequently observed. Figure 2B shows a highly magnified SEM image of a single *dried* pore of relatively large (~5 μm) diameter. Clearly apparent in this image are a large number of MSQ particles on the matrix surfaces (raised outer regions in the image) and within the pore. Such images prove that the MSQ nanoparticles described above exist within these films. The particles found on the matrix surface are all very small, having diameters of ~50 nm or less. In contrast, the particles found within the pore exhibit a broad distribution of sizes with the largest having ~200 nm diameters.

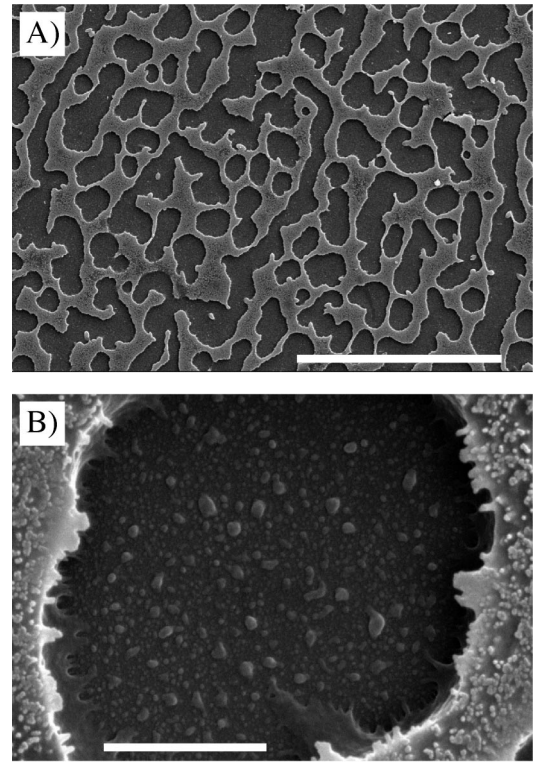

Figure 2. (A, B) Low- and high-magnification SEM images of the MSQ film used in the optical studies. The covering glass slide was removed well after gelation and aging (>35 h) to obtain these images. The pores (depressions), matrix (surrounding raised ridges), and small particles are clearly visible. Particles having a broad distribution of sizes are found within the pores. The largest particles observed in this region are ~200 nm in diameter. Particles of smaller average size are observed on the matrix. (A) Scale bar: 50 μm. (B) Scale bar: 2 μm.

Single Point CCS Studies of MSQ Film Evolution. While the optical images discussed above provide an initial view of overall MSQ film properties as well as the phase separation, gelation, and aging processes, detailed investigations of these materials in general and the properties of their solvent-filled pores in particular require implementation of altogether different methods. Here, confocal correlation spectroscopy (CCS)[21,30] provides valuable new data on the time evolution of the film properties in a spatially resolved fashion, by following time-dependent changes in the mobilities of MSQ nanoparticles found within the films. Previous studies have only reported on the static properties[1,19,20] and bulk dynamics[7,15] of related materials.

CCS involves the recording of time-dependent optical signals (i.e., time transients) from selected locations in the sample. As particles of sufficient size and appropriate optical properties migrate through the microscope focal volume, they produce "bursts" of scattered light. Autocorrelation of the time transients obtained provides the average time spent by the particles in the detection volume. The results yield information on the average size of the particles and/or the viscosity of the film region being probed. In the present studies, light scattering arises specifically from passage of MSQ nanoparticles through the detection volume. Interference from other regions of the film (i.e., static scattering by the matrix in gelled MSQ films) is virtually eliminated by the confocal nature of the method.

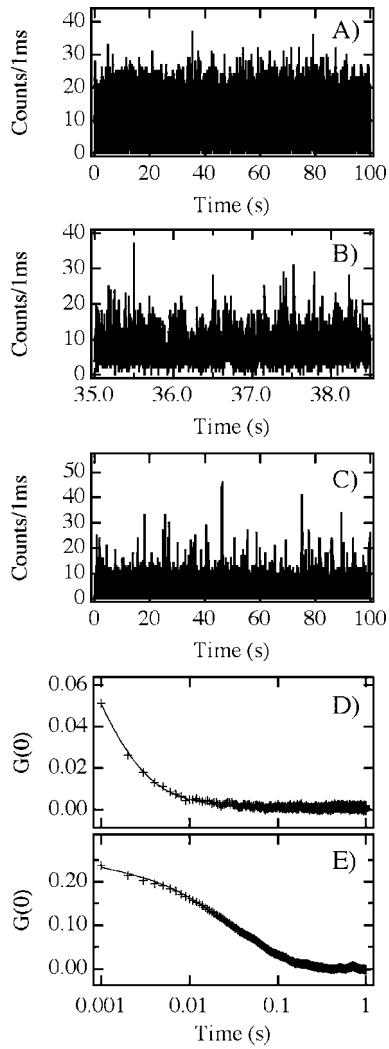

Figure 3. (A–C) Representative time transients and (D, E) associated autocorrelation functions obtained from the film/pores shown in Figure 1. (A, D) Data obtained at early times, prior to phase separation (70 min). (B) Expanded region of the transient shown in (A) and depicting signal fluctuations due to light scattering by small, mobile MSQ particles. (C, E) Data obtained at much later times (1000 min) also depicting scattering by MSQ particles. The longer autocorrelation decays observed at long times (compare D and E) reflect much slower, possibly hindered diffusion by larger MSQ particles in the pores of the film.

Representative time transients incorporating numerous bursts of scattered photons are shown in Figure 3A,C. Only the first 100 s of each transient is shown to better highlight the bursts, which are most clearly visible in Figure 3C. Figure 3B shows a greatly expanded section of the transient shown in Figure 3A for this same purpose. These time transients were obtained from single points in the film shown in Figure 1. In the case of Figure 3A,B the transient shown was obtained from a randomly selected position in the uniformly scattering film prior to phase separation. These data were obtained 70 min after sol preparation. The transient shown in Figure 3C was obtained by positioning *an individual pore* within the microscope focus after phase separation had occurred. This particular transient was obtained 16 h 40 min (1000 min) after sol preparation. Numerous such transients were recorded from this same sample over a period of ~35 h. The vast majority of transients were recorded with a time resolution of either 1 or 3 ms. In all cases, the transients were obtained from random positions prior to phase separation and from the pores after phase separation. Transients obtained from the matrix regions (not shown) yielded strong, constant (aside from shot noise) light scattering signals.

After each time transient was recorded, it was subsequently autocorrelated as follows:

$$G(\tau) = \frac{\langle I(t)\, I(t+\tau)\rangle}{\langle I(t)\rangle^2} - 1 \qquad (1)$$

In eq 1, $I(t)$ represents the time transient, τ is the discrete time base of the autocorrelation function, and the brackets $\langle\ \rangle$ indicate the average value over time is taken. Figure 3D,E depicts the autocorrelation functions obtained from the time transients shown in Figure 3A,C. As is obvious from Figure 3D,E, the average length of time the nanoparticles spend in the microscope detection volume increases dramatically with time, from ~1.1 ms at 70 min to ~50 ms at 16 h 40 min.

Quantitative data from these autocorrelation functions were obtained by fitting them to an approximate expression that models free (unhindered) diffusion of the nanoparticles in three dimensions. The results provide estimates of both the amplitude and rate of decay for each set of data. The specific equation employed in fitting the data was

$$G(\tau) = \frac{A_1}{(1 + D_1\tau/s^2)\sqrt{1 + D_1\tau/s_z^2}} + \frac{A_2}{(1 + D_2\tau/s^2)\sqrt{1 + D_2\tau/s_z^2}} + B \qquad (2)$$

Here, A_1 and A_2 represent the amplitudes of two distinct diffusional decays, while D_1 and D_2 represent the apparent diffusion coefficients for these two components. The parameter B is a constant used to properly fit the data, while s^2 and s_z^2 represent the transverse beam variance (determined elsewhere to be 2.6×10^{-10} cm^2)[23] and the longitudinal beam variance (assumed to be $2s^2$), respectively, at the microscope focus.

Prior to phase separation, virtually all of the data obtained could be fit to a single diffusional component (i.e., $A_2 = 0$ in eq 2). Such a result is consistent with a monomodal, random distribution of MSQ particle sizes. After phase separation, many of the autocorrelation functions showed clear evidence of a bimodal distribution of particles. As shown in Figure 3E, there is a dominant slow component to the decay and a small component (barely visible) associated with a faster decay. The latter decay occurs on a time scale very similar to that of the autocorrelation data obtained prior to phase separation.

The apparent D values obtained as a function of time provide valuable new insights into the evolution of the MSQ films. Figure 4A plots these data. Note that only the D values for the slow diffusional component are plotted in cases where a bimodal decay was observed. The fast component was frequently too small to yield results that could be quantitatively interpreted. In addition, the autocorrelation functions obtained between the phase separation and gelation times could not be reasonably fit to the above model. This is likely because of strong fluctuations in the local sample composition that occur during this time frame. These data have been excluded from Figure 4.

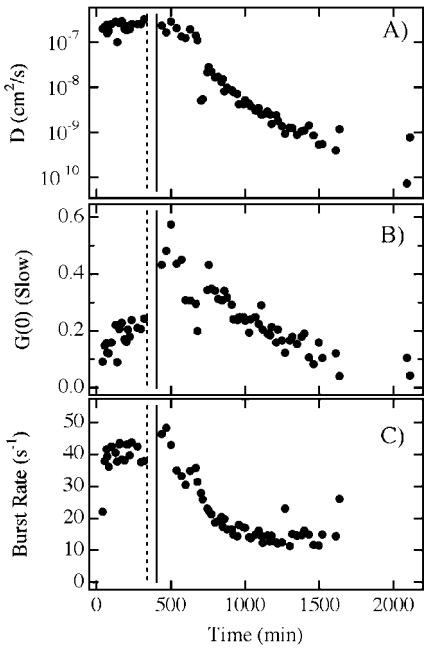

Figure 4. (A) Diffusion coefficient (slow component) as a function of time for MSQ particles found in the pores of the film shown in Figure 1. (B) Amplitude of the slow diffusion component. These data were obtained by fitting the autocorrelation functions to the equation described in the text. (C) Burst rate as a function of time. The vertical dashed line indicates the point at which phase separation occurred. The solid line depicts the time at which gelation of the bulk sample was observed. Data obtained near the phase separation and gelation times were excluded for the reasons discussed in the text. The last two points in (C) are not shown because these data were recorded using a longer bin time, yielding burst rates that were difficult to reconcile with the earlier data.

Aside from a couple of points at ~11.5 h, where the D values obtained were unexpectedly low, the results in Figure 4 can otherwise be roughly divided into two regions: those obtained before 10 h and those obtained afterward. Prior to 10 h, the apparent D values fluctuate around an average of $\sim 2 \times 10^{-7}$ cm^2/s. This result suggests the MSQ nanoparticles grow rapidly to a certain size but do not grow further until well after gelation. After 10 h (i.e., ~3 h after gelation), the apparent D values begin to decrease dramatically, suggestive of either a change in pore viscosity or a resumption of particle growth. This relatively long delay between gelation and the onset of changes in the apparent diffusion coefficient has been observed in several different experiments on different samples prepared and studied under the same (or very similar) conditions.

Regardless of the mechanism, it is clear that the average size of the particles detected remains approximately constant over the first 10 h. The average D value obtained may be used to estimate the average size of these particles. Assuming the particles are spherical in shape (see Figure 2), the Stokes–Einstein equation provides an estimate of the particle diameter. Here, $d = kT/(3\pi\eta D)$, where k is the Boltzmann constant, T is absolute temperature (293 K), and η is the viscosity of the liquid comprising the film. If the film behaves approximately like a mixture of water and methanol prior to phase separation and gelation, a viscosity of 0.8 cP may be assumed. With an average $D = 2 \times 10^{-7}$ cm^2/s, a particle diameter of ~26 nm is obtained. Note that this particle size corresponds reasonably well to the size of the particles observed on the matrix in Figure 2B.

The data shown in Figure 4 suggest particles of this size appear in the film very early, prior to collection of the first time transient. It is unlikely that the particles all grow rapidly to this size in the first few minutes. Rather, it is more likely that there exists a (broad) distribution of particle sizes and that only particles of a minimum size are being detected.

The minimum detectable particle size was estimated here using Mie scattering theory.[32] In making this estimate, it was assumed that only those particles producing signals equivalent to twice the background could be detected. The background count rate in these experiments was estimated to be ~3 ms^{-1}. Assuming a detection efficiency in the microscope of ~1% and an incident power of 3 μW, only those particles having backscattering cross sections of $>2 \times 10^{-16}$ cm^2 would produce detectable bursts. Assuming a refractive index of 1.33 for the sol and 1.4 for the MSQ particles formed at early times, one obtains a minimum detectable particle diameter of 34 nm from Mie theory.[32] Since conventional Mie theory assumes illumination by an infinite plane wave,[32] it is expected the minimum detectable particle size may be somewhat smaller in the microscope. It is therefore concluded that during the initial 10 h of data collection the MSQ nanoparticles take on a broad distribution of sizes, with the *detectable* particles growing to a size of ~30 nm.

The amplitude of the autocorrelation data provides strong evidence that smaller particles continue to grow to a size of ~30 nm prior to film gelation. Figure 4B plots these amplitudes (only the slow component is used for bimodal decays) as a function of time. Prior to phase separation and gelation, the amplitude of the autocorrelation decay increases steadily in time. As has been shown previously,[33,34] for background-limited detection of single particles, the autocorrelation amplitude exhibits a complicated dependence on particle concentration. However, at the lowest concentrations, the amplitude may be assumed to increase linearly with concentration. Therefore, these data suggest that while the particles grow no larger than ~30 nm at early times, the number of such particles of this size is continuously increasing. The increase in autocorrelation amplitude may also reflect densification of the silica particles, producing particles that have a greater refractive index and more strongly scatter the incident laser light. In either case, these results point to the continued evolution of the MSQ nanoparticles, namely via formation of Si–O–Si bonds. The gradual rise in the optical density of the bulk sample (see Figure 1) prior to phase separation is also consistent with this conclusion: either the number of particles present is increasing or their light scattering efficiency is increasing. Shortly after phase separation and gelation (at 410 min), the autocorrelation amplitude begins to decrease, indicative of a time-dependent decrease in the concentration of nanoparticles within the pores. Note that this behavior contrasts with the time-dependent D values obtained in that the D values

(32) Born, M.; Wolf, E. *Principles of Optics*; Cambridge University Press: Cambridge, 1998.
(33) Koppel, D. E. *Phys. Rev. A* **1974**, *10*, 1938–1945.
(34) Ye, F.; Collinson, M. M.; Higgins, D. A. *Anal. Chem.* **2007**, *79*, 6465–6472.

remain approximately constant for a long period of time (~3 h) after gelation, suggesting little or no growth of detectable particles is occurring.

Because of the complex dependence of the autocorrelation amplitude on concentration changes,[33,34] the burst rate (i.e., number of bursts per second) observed in each transient was also calculated from the time transient data and used as a means to observe changes in the particle concentration. The observed burst rate is also expected to be proportional to, among other things, the concentration of detectable particles present, assuming their concentration is sufficiently low. The burst rate was obtained by first determining the average background count rate in each transient. All bursts for which the signal exceeded the background fluctuations at the 99.9% probability level (assuming the background is Poisson distributed) were then counted. Figure 4C plots the results obtained. As with the autocorrelation amplitude data, the burst rate increases up until phase separation and gelation, consistent with an increase in the concentration of 30 nm particles during this time. As with the autocorrelation amplitude and in contrast to the *D* values, the burst rate data also begin to decrease shortly after gelation of the film, suggestive of the onset of a monotonic time-dependent decrease in the number of particles present within the pores. Taken together, the observed changes in the autocorrelation amplitude and the burst rate provide strong evidence for a decrease in the nanoparticle concentration after gelation.

Interpretation of CCS Results and Proposed Nanoparticle Growth Mechanism. The nanoparticle growth, phase separation, gelation, and aging processes are all very complicated, involving chemistries that varying substantially in time. The relevant processes that are believed to occur are described below for the different time periods involved in the evolution of these materials.

I. Prior to Phase Separation. The initial growth mode likely involves reactions between monomers and small MSQ oligomers. Unfortunately, this early phase of oligomer growth cannot be followed in the present studies because the structures formed are too small to be detected. However, these processes have been investigated previously in related materials by NMR.[11,14,16,17,35]

Under the conditions employed in MSQ synthesis (pH ~ 1 and Si:water ratio 1:2), hydrolysis of MTMOS is expected to be very rapid.[11,14,35] The hydrolyzed monomeric species thus produced then condense to form dimers, trimers, and other small linear and cyclic oligomers. Condensation in these materials may occur between neutral and protonated silanol groups.[36,37] As has been suggested previously, the least condensed MSQ species are expected to incorporate the most basic silanols while the most condensed species are most acidic.[36,37] Steric effects may also play a significant role,[17] with early reactions preferentially occurring between weakly condensed species. As the monomers are consumed, the growth mechanism becomes dominated by reactions between larger oligomers (sterically hindered species that may also incorporate neutral silanols) and smaller oligomers (unhindered species incorporating protonated silanols). As larger polymers are formed, they become visible in the CCS experiments. At the same time, the particle growth rate slows dramatically because the concentration of reactive small species decreases as they are incorporated into larger structures and because of the reduced reactivity (i.e., decreased basicity and increased steric hindrance) of the silanols present on relatively large MSQ polymers. Particle growth by interparticle aggregation is also unlikely at this point because of reduced surface reactivity, increased steric hindrance, and a reduction in the rate of particle diffusion (and hence particle collisions) as the particles grow. This decline in particle growth rate becomes most noticeable at times close to phase separation/gelation. In the present experiments, this growth process results in the production of nanoparticles having a maximum size of ~30 nm. Particle size remains (temporarily) stable after this point.

II. Phase Separation/Gelation. While particle growth is interrupted for the above reasons, intraparticle condensation continues to occur. The nanoparticles densify in time and also become less polar. A decrease in polarity results from the time-dependent decrease in silanol density. At some point in time, a critical concentration of nonpolar species is reached and phase separation occurs, forming a two-phase system incorporating regions of high (the "matrix phase") and low (the "pore phase") MSQ concentrations. The least polar, most highly condensed species dominate in the high concentration regions, while the low concentration regions are comprised primarily of solvent but also incorporate the most polar, least condensed nanoparticles.

Aggregation of the least polar MSQ species in the matrix phase and subsequent condensation of their residual silanol groups leads to gelation of the matrix. In contrast, in the pore phase, the concentration of nanoparticles is relatively low, interparticle collisions are infrequent, and the nanoparticles themselves remain predominantly nonreactive toward each other. The least polar of these particles can still react with and become incorporated in/on the matrix. This process is reflected by the decrease in particle concentration observed shortly after matrix gelation in the autocorrelation amplitude and burst rate data shown in Figure 4.

III. After Gelation. In time, the condensation reactions occurring within the pore-phase nanoparticles cause them to become sufficiently nonpolar that they begin to aggregate and react with each other. A resumption of particle growth in the individual pores is then observed. In these particular materials, this process requires an additional ~3 h after phase separation, as reflected by the delayed onset of the decrease in *D* shown in Figure 4.

As noted above, the decrease in *D* after 10 h is consistent with either the resumption of particle growth or a change in the viscosity of the liquid-filled pores. The latter mechanism is discounted on the basis of the observation of two-component diffusion within the pores at these later times. The fast diffusional components in many of the autocorrelation decays yield apparent *D* values similar to those obtained at early times, prior to phase separation. This result

(35) Alam, T. M.; Assink, R. A.; Loy, D. A. *Chem. Mater.* **1996**, *8*, 2366–2374.
(36) Iler, R. K. *The Chemistry of Silica*; John Wiley and Sons: New York, 1979.
(37) Brinker, C. J.; Scherer, G. W. Sol-Gel Science. *The Physics and Chemistry of Sol-Gel Processing*; Academic Press: Boston, 1990.

suggests that some smaller particles remain in the pores over very long periods of time. Regardless of the origins of these small particles, their relatively fast diffusion indicates that the viscosity of the liquid-filled pores has not changed substantially. It is therefore concluded that the drop in D observed after 10 h results entirely from particle growth by an aggregation mechanism.

The Stokes–Einstein equation again provides a means to estimate particle size as nanoparticle growth resumes. All such estimates assume the viscosity of the liquid filled pores remains approximately constant. The particles apparently grow from the initial minimum detectable size of ~30 nm to diameters of ~300 nm after only 3 h of additional aging (beyond 10 h). Only a few hours later, the D values obtained suggest unrealistically large particles of >3 μm average diameters. The SEM results described above suggest that the particles do not grow significantly beyond a few hundred nanometers in size. The observed decrease in D is thus concluded to reflect the onset of strongly hindered nanoparticle diffusion within the MSQ pores. It is well-known that once the particles grow to sizes larger than ~10% of the pore size, the D values obtained will fall precipitously from those expected for free diffusion.[38] As may be estimated from the optical images shown in Figure 1, the pores investigated in these studies are at most a few micrometers in diameter, indicating hindered diffusion should become important as the particles grow to diameters of only a few hundred nanometers.

As a final caveat, it should be noted that the SEM images shown in Figure 2 provide support for the above particle growth mechanism. The particles trapped on the matrix are all observed to be of relatively small size (~50 nm or less in diameter). In contrast, those found within the pores take on a broad range of sizes from very small to as large as a few hundred nanometers. As defined in the above mechanism, the particles found on the matrix surfaces were likely deposited after phase separation and gelation had occurred but prior to the onset of nanoparticle aggregation. Therefore, they remain smaller in size. In contrast, the particles found in the matrix had the opportunity to grow further by particle aggregation and are observed to be larger as a result.

(38) Beck, R. E.; Schultz, J. S. *Science* **1970**, *170*, 1302–1305.

Conclusions

Optical microscopy was used to directly observe phase separation and gelation in macroporous MSQ films formed from MTMOS under low pH conditions. When coupled with in situ single-site confocal correlation spectroscopy and scanning electron microscopy, valuable information on film morphology and the growth of MSQ nanoparticles in the liquid-filled pores of the MSQ matrix was obtained. It was found that the MSQ nanoparticles grew to a maximum diameter of ~30 nm soon after film preparation and remained in this size range until well after gelation. Nanoparticle size stabilization was attributed to consumption of reactive MSQ species, to a condensation-induced decrease in nanoparticle surface reactivity, and to a decrease in the collision rate of the MSQ particles as they grow. Incorporation of some nanoparticles in/on the matrix commenced shortly after gelation, as evidenced by a time-dependent decrease in the number of particles present in the pores. In contrast, the onset of particle–particle reactions within the individual pores was delayed for ~3 h after gelation, at which time a significant time-dependent decrease in the nanoparticle diffusion coefficient was observed. Nanoparticle growth in this later phase was attributed to particle aggregation after a further evolution of their properties.

The ability to probe macroporous sol–gel-derived films at the single pore level by optical microscopic methods will pave the way to a deeper fundamental understanding of the phase separation, gelation, and aging processes in these technologically important materials. Extensions of these methods will also allow for a better understanding of phenomena such as hindered diffusion within the macropores and molecule–matrix interactions in chemical or biomolecule separations.

Acknowledgment. The authors gratefully acknowledge the support of the National Science Foundation (CHE-0316466, CHE-0647849, and CHE-0648716) in these studies. Prof. Chris Sorenson is thanked for helpful discussions on the light scattering measurements.

CM702382C